

Design of Novel Rho Kinase Inhibitors Using Energy Based Pharmacophore Modeling, Shape-Based Screening, in Silico Virtual Screening, and Biological Evaluation

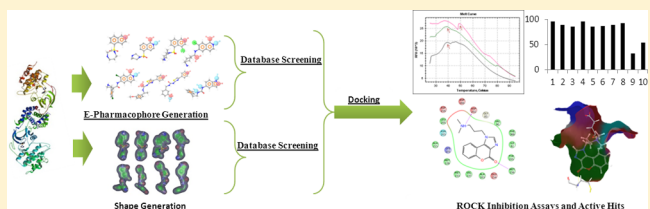
Ram Kumar Mishra,[†] Reshma Alokam,[†] Sarthak Mohan Singhal,[†] Geethasai Srivathsav,[†] Dharamarajan Sriram,[†] Neerja Kaushik-Basu,^{*,‡} Dinesh Manvar,[‡] and Perumal Yogeeshwari^{*,†}

[†]Computer-Aided Drug Design Lab, Department of Pharmacy, Birla Institute of Technology & Science–Pilani, Hyderabad Campus, Jawahar Nagar, Hyderabad–500078, Andhra Pradesh, India

[‡]Department of Microbiology, Biochemistry and Molecular Genetics, Rutgers, The State University of New Jersey, New Jersey Medical School, 185 South Orange Avenue, Newark, New Jersey 07103, United States

Supporting Information

ABSTRACT: Rho-associated protein kinase (ROCK) plays a key role in regulating a variety of cellular processes, and dysregulation of ROCK signaling or expression is implicated in numerous diseases and infections. ROCK proteins have therefore emerged as validated targets for therapeutic intervention in various pathophysiological conditions such as diabetes-related complications or hepatitis C-associated pathogenesis. In this study, we report on the design and identification of novel ROCK inhibitors utilizing energy based pharmacophores and shape-based approaches. The most potent compound **8** exhibited an IC₅₀ value of 1.5 μM against ROCK kinase activity and inhibited methymercury-induced neurotoxicity of IMR-32 cells at GI₅₀ value of 0.27 μM. Notably, differential scanning fluorometric analysis revealed that ROCK protein complexed with compound **8** with enhanced stability relative to Fasudil, a validated nanomolar range ROCK inhibitor. Furthermore, all compounds exhibited ≥96 μM CC₅₀ (50% cytotoxicity) in Huh7 hepatoma cells, while 6 compounds displayed anti-HCV activity in HCV replicon cells. The identified lead thus constitutes a prototypical molecule for further optimization and development as anti-ROCK inhibitor.



1. INTRODUCTION

Rho-associated protein kinase (ROCK) aka Rho-associated, coiled-coil-containing protein kinase is a serine-threonine kinase and a downstream effector of RhoA. Two isoforms of ROCK are known: ROCK-I (ROCK-β) and ROCK-II (ROCK-α).¹ ROCK plays an important role in a variety of cellular processes such as stress fiber formation, focal adhesion, aggregation, cell morphology, migration, and proliferation.^{2,3} Dysregulation of ROCK activity or expression has been linked with diseases like hypertension,⁴ stroke,⁵ glaucoma,⁶ and cancer.⁷ Notably, the RhoA/ROCK pathway has been implicated in several diabetes-associated complications such as retinopathy and inflammation,⁸ nephropathy,⁹ erectile dysfunction,¹⁰ and neuropathy, among others.¹¹ Thus, small molecule ROCK protein inhibitors like Fasudil, Hydroxyfasudil, H-1152P, and Y-27632 (Figure 1) are being extensively used in both research and clinical trials.¹² ROCK inhibitors have also found application as probes to investigate hepatitis C virus (HCV)-associated pathogenesis mechanisms. For instance, the significance of HepG2 polarization in limiting HCV entry was demonstrated by treating cells with protein kinase A agonist, oncostatin M in the presence of ROCK inhibitor Y-27632.¹³ Another study utilized the ROCK inhibitor Hydroxyfasudil along with Fluvastatin to demonstrate the negative impact of

matrix stiffness on HCV replication.¹⁴ These findings implicate ROCK proteins as potential targets for drug-discovery against HCV-associated hepatocellular carcinoma. Thus, design of potent ROCK inhibitors against multiple diseases has received widespread attention in the scientific community. Thus, cocrystal structures of ROCK proteins bound to four different ATP-competitive inhibitors (Y-27632, Fasudil, Hydroxyfasudil, and H-1152P) have been determined.¹⁵ These high resolution structures have paved the way for structure-based ROCK inhibitor design and molecular dynamics simulations and provide an extensive mapping of potential small-molecule binding pockets on Rho family members.¹⁶ Fragment-based screening assisted by structure-guided design has also been employed toward the identification of selective ROCK-I and ROCK-II inhibitors.¹⁷

In the present study, we describe the identification of diverse ROCK inhibitor scaffolds by structure-guided design integrating multiple cocrystal structures of ROCK-inhibitor complexes. Further, energy-based pharmacophore and shape-based modeling of eight crystal structures of ROCK proteins in complex with inhibitors was achieved and utilized as filters in the virtual

Received: July 31, 2014



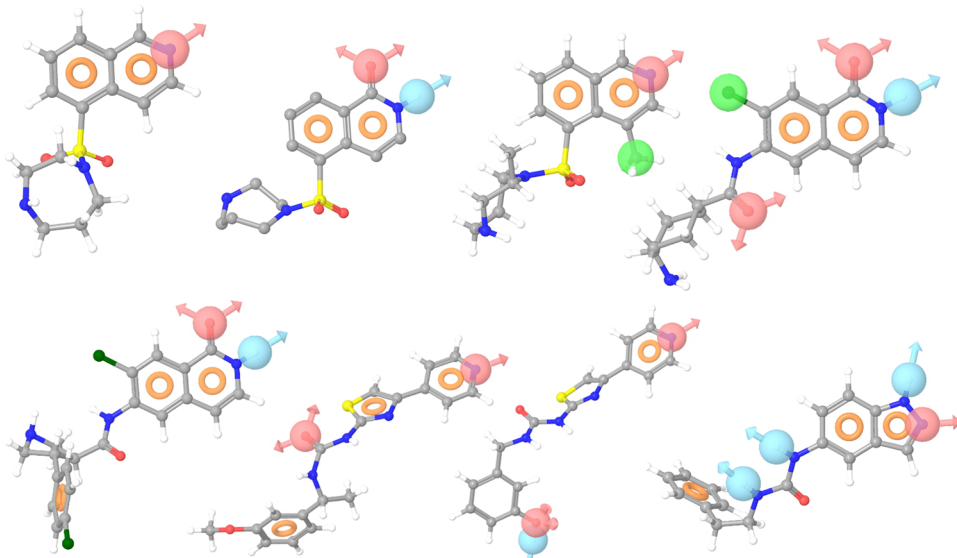


Figure 1. Energy based pharmacophores. E-pharmacophores derived from the crystal structures (left to right, top row: 2ESM, 2ETK, 3D9V, and 3NCZ; bottom row: 3NDM, 3TV7, 3TWJ, and 3V8S). In general, pharmacophoric sites can be represented as six chemical features viz. hydrogen bond acceptor (A), hydrogen bond donor (D), hydrophobic (H), negative ionizable (N), positive ionizable (P), and aromatic ring (R). Pharmacophoric features have been depicted in different shapes and colors; pink sphere denote acceptor atom feature; cyan sphere, donor atom feature; green sphere, hydrophobic feature whereas orange donuts represent aromatic feature. Ligand atoms have been shown as a ball and stick model. The figures were generated in Maestro.

screening protocol. The proof of concept for the design strategy was performed utilizing various biological assays, and we report herein the results of our studies to identify novel ROCK inhibitors. The method combines pharmacophore perception along with shape complementarity and database screening with protein–ligand energetic terms computed by the Glide XP (extra precision) scoring function, as we believe that integration of multiple crystal structure information is fruitful as envisaged successfully in our earlier work with β -secretase and HCV NS5B.^{18,19}

2. MATERIALS AND METHODS

2.1. Computational Details. All computations were carried out on an Intel Core 2 Duo E7400 2.80 GHz capacity processor with a memory of 2 GB RAM running with the RHEL 5.2 operating system. Glide 5.7 module of Schrödinger suite was used to screen Asinex database. Phase 3.3 implemented in the Maestro 9.3 software package (Schrödinger, LLC) was used to generate pharmacophore.

2.2. Protein Structure Preparation. We selected eight crystal structures of ROCK I bound with inhibitors from PDB that included 2ESM, 3D9V, 2ETK, 3NCZ, 3NDM, 3TV7, 3TWJ, and 3V8S. Protein preparation wizard in Maestro software was used to prepare the proteins (Maestro, v9.2, Schrodinger, LLC, New York, NY). Co-crystallized water molecules beyond 5 Å of bound inhibitor were removed. Proteins were minimized using OPLS_2005 force field. Bond orders and formal charges were added for hetero groups, and missing hydrogen atoms were added to correct the ionization and tautomeric states of amino acid residues (see the Supporting Information).

2.3. Energy-Optimized Structure-Based Pharmacophore Hypothesis Generation. Energetic descriptions of the ligand–receptor complexes were retrieved using G scoring function which is part of docking program Glide 5.7.²⁰ The procedure followed was as reported earlier by our group.¹⁹

Briefly, based on the XP descriptor information pharmacophore features were generated using Phase 3.3 using the default set of six chemical features: hydrogen bond acceptor (A), hydrogen bond donor (D), hydrophobe (H), negative ionizable (N), positive ionizable (P), and aromatic ring (R). Hydrogen bond acceptor sites were represented as vectors along the hydrogen bond axis in accordance with the hybridization of the acceptor atom. Hydrogen bond donors were represented as projected points, located at the corresponding hydrogen bond acceptor positions in the binding site. Each pharmacophore feature site was first assigned an energetic value equal to the sum of the Glide XP contributions of the atoms comprising the site, allowing sites to be quantified and ranked on the basis of the energetic terms. ChemScore, hydrogen bonding, and lipophilic atom pair interaction terms were included when the Glide XP terms for hydrogen binding and hydrophobic enclosure were zero.

2.4. E-Pharmacophore Validation. E-pharmacophores were validated using receiver operating characteristics (ROC) calculations. ROC represented a plot of true positive rate as a function of the false positive rate.²¹ AUC, the area under the ROC curve, represented quantification of the curve. Thus, AUC facilitated an easier comparison of results. AUC was calculated as follows:

$$\text{AUC} = 1 - \frac{1}{N_{\text{active}}} \sum_i^{N_{\text{active}}} \frac{N_{\text{decoys seen}}^i}{N_{\text{decoys}}}$$

where N_{active} depicted the number of actives, N_{decoys} represented the number of decoys, and $N_{\text{decoys seen}}^i$ described the number of decoys ranked higher than the i th active structure. AUC range between 0 and 1 and a value of 0.5 indicated a random performance. AUC metric could be considered as a measure to evaluate the performance on the complete data. However, additional matrices were also needed to retrieve actives from a small fraction of database. To solve this problem, the

enrichment factor at a predefined fraction of the data set ($x\%$) was calculated as follows:

$$\text{EF}_{x\%} = \frac{\frac{N_{actives\ seen}}{N_{x\%}}}{\frac{N_{actives}}{N_{actives} + N_{decoys}}}$$

The enrichment factor depended on the number of actives, and therefore it was not a robust metric. Another popular metric for the early enrichment evaluation was the Boltzmann-enhanced discrimination of receiver operating characteristic (BEDROC) score. All eight e-pharmacophores were checked for the enrichment factor (EF), BEDROC ($\alpha = 160.9, 20$, and 8), based on recovery rate of actives against the ranked decoy database. ROC was calculated by screening a database consisting of 35 known inhibitors reported elsewhere²² and 1000 drug-like ligand decoys set available at Schrodinger. Manual EF (EF_{manual}) and goodness of hit (GH) values were calculated using the following formulas:

$$\text{EF}_{\text{manual}} = \frac{H_a \times D}{H_t \times A}$$

$$\text{GH} = \left(\left(\frac{H_a}{4H_t A} \right) \times (3A + H_t) \right) \times \left(1 - \frac{H_t - H_a}{D - A} \right)$$

where H_t represented the number of hit molecules from the database, H_a was the number of active molecules in hit list, D was number of decoys and A was the number of actives.

2.5. Molecular Shape-Based Screening. All the PDBs utilized for e-pharmacophore generation were also employed for molecular shape analysis after preparing the protein. The query was prepared using default Omega parameters and ImplicitMillsDean force field. Molecular shape and color atoms were automatically assigned to the query. One query was generated from each prepared PDB structure.

2.6. Shape Validation. Each query was validated using a directory of useful decoys (DUD) data set.²³ Actives used in e-pharmacophore validation were also used for shape validation. The “perform ROCS validation” script in ROCS was used for shape validation. Decoys and active databases were prepared using Omega with default settings. AUC for the ROC curve and enrichment at 0.5% , 1% , and 2% were calculated. Based on AUC and enrichment factors, final shapes were selected for further studies.

2.7. E-Pharmacophore and Shape-Based Virtual Screening. The commercially available Asinex database containing $525,807$ molecules was used for virtual screening. The database was prepared using the LigPrep 2.5²⁴ module of the Schrodinger suite. The Phase 3.3 module of the Schrodinger suite was employed for database screening. Each e-pharmacophore was individually subjected to a database search using the “find matches” option. The database was screened with the following conditions: (a) conformation of the database molecules was generated on the fly by implementing flexible search, (b) at least three of the four sites of the quantitative common pharmacophore should be matched, and (c) it should not consider partial matches involving more sites. Output from all database screening runs was merged and duplicates were identified. Among duplicates, only the molecules with the highest fitness score were retained. Finally, 12756 molecules with fitness ≥ 2 were selected for docking.

For the shape based filtering the Asinex database was prepared using the Omega 2.3.2²⁵ module in Open Eye Systemic Software. The final selected shapes were subjected to database screening. Hits were pooled and sorted by Tanimoto combo rankings. Duplicates were identified, and only those with the highest Tanimoto scores were retained. Top molecules with high Tanimoto scores were selected as hits for further studies.

2.8. Molecular Docking. Filtered hits from e-pharmacophore and shape-based screening were subjected to docking studies into the respective crystal structure active sites. Three modules of Glide were used for docking: high throughput virtual screening (HTVS), followed by standard precision mode (SP) and extra precision mode (XP). Glide HTVS is faster and more tolerant to suboptimal fits than Glide XP, making it better for comparison in this work.²⁶ The center of the Glide grid was defined by the position of the cocrystallized ligand. Default settings were used for both the grid generation and docking. Postdocking minimization was implemented to optimize the ligand geometries. Compounds with best docking and Glide scores were then subjected to Glide SP and XP screening. Finally we identified top ranked molecules based on docking score and visual inspection. ADME properties of the top ranked molecules were calculated using the QikProp²⁷ module of the Schrodinger suite.

2.9. In Vitro Rho Kinase Inhibition Studies. Top hits were procured from Asinex. The cloned ROCK construct pET-21d Rho kinase was obtained from our collaborator at the National Institute of Immunology, New Delhi, India. HEK 293 cells were procured from the National Center for Cell Sciences, Pune, India, and IMR-32 cells were gifted by the Center for Cellular and Molecular Biology, Hyderabad, India. Methyl-mercury (MeHg) was obtained from Sigma-Aldrich, India. Other supplies were procured from Sigma-Aldrich or Himedia.

2.10. Expression and Purification of ROCK. Plasmid pET-21d Rho kinase was transformed in *E. coli* BL21(DE3) and used for purification of ROCK-I. This plasmid carries a hexahistidine tag (His-Tag) at its N-terminus which facilitates purification by Ni-NTA affinity chromatography. The protein was induced at $18\text{ }^{\circ}\text{C}$ for 16 h by addition of 0.1 mM isopropylthio- β -galactoside. Cell pellet was homogenized in lysis buffer containing 10 mM Na_2HPO_4 , 1.8 mM KH_2PO_4 , pH 7.4 , 137 mM NaCl , 2.7 mM KCl , 1 mM DTT, protease inhibitors cocktail (Sigma Cat. NO P8465), and 5% glycerol (PBSG), sonicated, and centrifuged at $10,000$ rpm for 35 min . The clarified lysate was mixed with pre-equilibrated Ni-NTA resin and gently twirled at $4\text{ }^{\circ}\text{C}$ for $3^{1/2}\text{ h}$ for facilitating binding of the His-Tag protein. The resin bound protein was centrifuged at 500 rpm for 5 min , packed on a Biorad column in PBSG, and bound protein eluted stepwise with TBG elution buffer (50 mM Tris-HCl pH 7.4 , 137 mM NaCl , 2.7 mM KCl , and 5% glycerol) containing 0 , 10 , 25 , 50 , 100 , or 200 mM imidazole, and monitored by the Bradford colorimetric assay. The purity of ROCK-I was determined by Coomassie-blue stained SDS-PAGE analysis. Fractions enriched in ROCK-I ($>95\%$ purity) were pooled and dialyzed against TBG containing 50% glycerol, divided into aliquots and stored at $-80\text{ }^{\circ}\text{C}$.

2.11. Inhibition of ROCK Kinase Activity. Inhibition of ROCK kinase activity was evaluated spectrophotometrically in a coupled assay format, wherein a molecule of NADH is oxidized to NAD⁺ each time a phosphate is transferred by ROCK.²⁸ The assay was conducted in a 96-well plate format in

Table 1. Distance between E-Pharmacophores Features^a

s. no.	PDB	distance between features (Å)								
		R1-R2	R1-A1	R2-A1	R1-H1	R2-H1	A1-H1	R1-D1	R2-D1	A1-D1
1	2ESM	2.452	3.734	1.413						
2	2ETK	2.471	3.728	2.676				4.708	2.389	2.496
3	3D9V	2.457	3.731	1.417	4.024	2.916	3.757			
4	3NCZ	2.462	3.731	2.678				4.697	2.379	2.505
5	3NDM	2.461	3.714	2.681				4.694	2.385	2.516
6	3TV7	4.18	5.54	1.36						
7	3TWJ			1.421						
8	3V8S		3.332	1.15				3.451	2.146	2.112

^aR: aromatic ring, A: acceptor, H: hydrophobic, D: donor.

a reaction mix (90 µL) containing 0.1 M HEPES (pH 7.6), 10 mM MgCl₂, 2.5 mM PEP, 0.2 mM NADH, 0.01 mg/mL LDH, 2 mM DTT, 100 nM of ROCK protein, and 100 µM MBP (myelin basic protein) as the universal kinase substrate. Reaction was initiated by addition of 10 µL of 30 µM ATP and absorbance measured at 340 nm in a multiplate reader (PerkinElmer Victor V3 spectrophotometer). Preliminary screening was conducted at 40 µM compound concentration, and active compounds were further investigated in a dose-response assay for 20 of their IC₅₀ values, which was computed using GraphPad prism 5.03 software (La Jolla, CA, USA).

2.12. Differential Scanning Fluorimetry (DSF) Experiments. The ability of compounds to bind and stabilize ROCK was further investigated using the DSF technique.²⁹ ROCK protein was stepwise heated alone, with Fasudil or the most active lead compound from 20 to 100 °C in the presence of the fluorescence dye (SYPRO orange). Upon heat-denaturation, the fluorescence of SYPRO orange increases while interacting with the hydrophobic residues. Fluorescence was measured three times per minute using a LED/photodiode set matched to the excitation and emission wavelengths of SYPRO orange. The recorded fluorescence readings were fitted to the Boltzmann sigmoid function using CFX Manager software 3.0. Melting point of the protein was obtained as the lowest point of first derivative plot. Melting temperature (*T*_m) was defined as the inflection point of each fitted curve. The observed temperature shift, Δ*T*_m, was recorded as the difference between *T*_m of a sample and a reference in the same plate. The data was processed, and *T*_m values were calculated by fitting to the Boltzmann equation.

2.13. Cell Culture. HEK 293 and IMR-32 cells were utilized for the cell based assays. The cells were cultured in MEM medium supplemented with FBS (10%), L-glutamine (1%), penicillin (10,000 units), and streptomycin (10 mg/mL) at 37 °C in 5% CO₂ atmosphere. For all assays, cells were maintained at 90% confluence and used as required. MeHg (10 mM) was prepared in double distilled water and further diluted as per requirement. All inhibitors were dissolved in DMSO (10%).

2.13.1. Cytotoxicity Studies. MTT ((3-(4,5-dimethylthiazol-2-yl)-2,5-diphenyltetrazolium bromide) reduction assay was used to measure cytotoxicity.³⁰ Briefly, exponentially growing HEK 293 cells (10,000 cells/well) seeded in a 96-well plate in MEM medium containing 1% FBS were treated with 100 µM compound for 48 h. For cell viability evaluations, 10 mg/mL of MTT solution in 1X PBS was added to the wells and incubated for 3 h. The violet crystals formed were dissolved in 100% DMSO and absorbance measured at 595 nm in spectrophotometer (PerkinElmer victor X3). The experiment was done in triplicates, and percent cytotoxicity was calculated.

2.13.2. Growth Inhibition Assay. Inhibition of growth of the IMR-32 cells by the eight compounds was measured in a dose-response curve in triplicate. Approximately 5000 cells per well were utilized for this investigation, and growth inhibition was measured by MTT addition, similar to the cell cytotoxicity studies. GI₅₀ values were calculated using GraphPad prism 5.03.

2.13.3. Measurement of Reactive Oxygen Species (ROS) Production. Intracellular ROS estimation was measured using DCFH-DA.³¹ Approximately 5000 IMR-32 cells per well were plated in a 96 well plate, treated with 5 µM DCFH-DA for 1 h followed by 20 µM MeHg for 2 h. Compounds were added at varying concentrations for 3 h, fresh medium replenished, and cells cultured further for 24 h. Oxidized DCFH excitation and emission was measured at 485 and 525 nm, respectively, in a spectrophotometer (SpectraMax M4, Molecular Devices, Sunnyvale, USA). Fasudil was employed as a positive control. Percent ROS production inhibition was calculated using GraphPad prism 5.03.

2.13.4. Clonogenic Assay. Clonogenic assay or colony formation assay is an *in vitro* cell survival assay which is based on the ability of a single cell to grow into a colony. Approximately 1000 cells per well were plated in a 12 well plate. Cells were treated with 20 µM MeHg for 2 h and incubated with 50 µM compounds for 3 h. The cells were replenished with fresh medium and incubated for 14 days. Fasudil was used as control. Plating efficiency (PE) and survival fraction (SF) were calculated as follows:³²

$$PE = \frac{\text{Number of colonies counted}}{\text{Number of cells plated}} \times 100$$

$$SF = \frac{PE \text{ of treated sample}}{PE \text{ of control}} \times 100$$

2.14. Statistical Analysis. The significance of the differences between treatments and respective controls was analyzed using one-way analysis of variance and with Bonferroni's post hoc test using GraphPad Prism. The data is presented as mean ± SEM.

2.15. Anti-HCV Activity and Cytotoxicity in Cell-Based Assays. Anti-HCV activity of compounds in cell based assays was investigated in Huh7/Rep-Feo1b and Huh7.5-FGR-JC1-Rluc2A cells, which carry the autonomously replicating HCV RNA of genotypes 1b and 2a in the firefly and *Renilla* luciferase reporters, respectively.^{19,33–35} In brief, the cells were grown in 96 well plates and treated with the compound (50 µM) or equal amounts of DMSO (control). After 48 h of treatment, cells were washed with phosphate buffered saline, and the effect of compounds on HCV RNA replication was measured as the relative levels of the luciferase signals in compound treated cells

Table 2. E-Pharmacophore Validation

PDB	e-pharmacophore	EF (%)	BEDROC ($\alpha = 160.9$)	BEDROC ($\alpha = 20.0$)	BEDROC ($\alpha = 8.0$)	ROC	RIE	AUC	EF (manual)	GH
2ETK	ADRR	29	0.075	0.601	0.728	0.99	8.74	0.87	10.902	0.469
2ESM	ARR	21	0.649	0.778	0.791	1.00	11.30	0.99	10.256	0.444
3D9V	AHRR	15	0.53	0.69	0.83	0.98	9.97	0.96	4.329	0.289
3NCZ	AADHRR	3	0.11	0.04	0.03	1.02	0.54	1	5.714	0.156
3NDM	ADRRR	15	0.48	0.76	0.79	1.00	11.10	0.98	14.285	0.558
3TV7	AARRR	0	0.00	0.06	0.13	0.98	0.88	0.96	0.823	0.060
3TWJ	AADR	0	0.01	0.08	0.10	1.01	1.21	1.00	2.077	0.078
3V8S	ADDDR	8.9	0.37	0.12	0.10	1.02	1.67	1.00	14.285	0.395

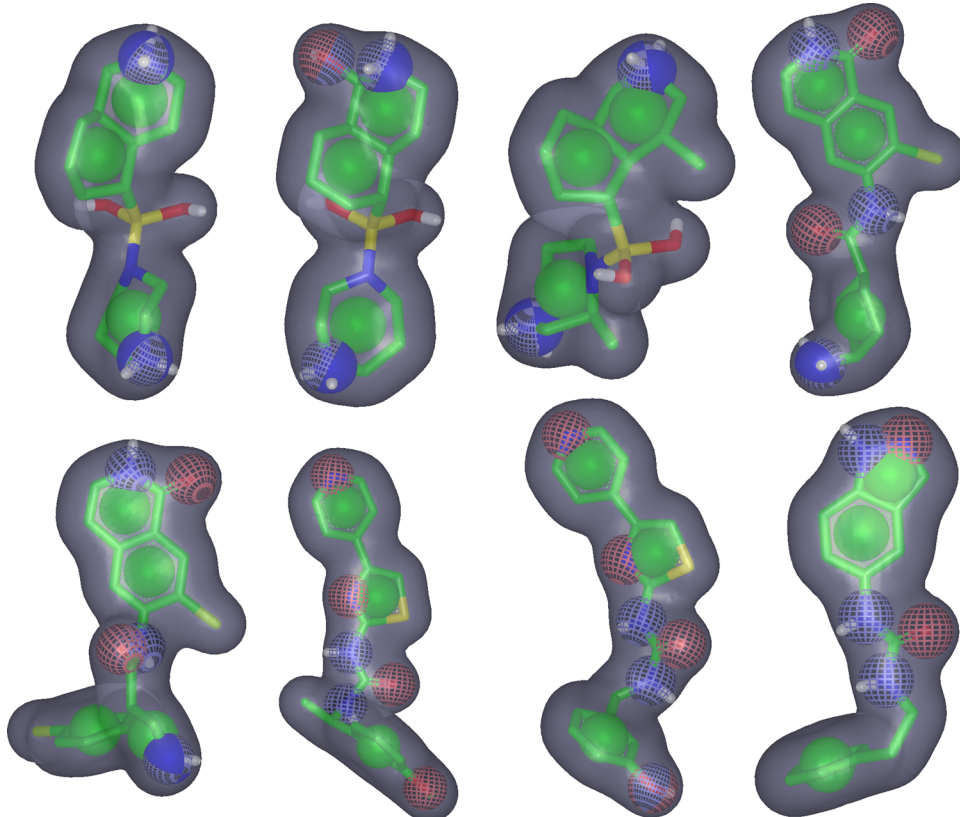


Figure 2. Shape based queries generated from the eight crystal structures (left to right, top row: 2ESM, 2ETK, 3D9V, and 3NCZ; bottom row: 3NDM, 3TV7, 3TWJ, and 3V8S).

versus DMSO controls employing a luciferase assay system (Promega). The effect of the compounds on cell viability was investigated in the parental Huh7 cells employing CellTiter 96 AQueous One solution in accordance with the manufacturer's protocol (Promega, USA). Briefly, cells seeded in 96 well plates were treated with 8 serial dilutions of the compound or DMSO for 48 h and 50% cytotoxic concentration (CC_{50} value) was derived from dose-response curves.

3. RESULTS AND DISCUSSION

As our drug design strategy was based on a structure-based approach, it was important to employ the crystal structure of ROCK bound to the inhibitor. In this work we selected eight cocrystal structures from the protein databank (pdb; <http://www.rcsb.org/pdb>) of ROCK-bound with ligands and having resolutions from 2.29 to 3.30 Å. Protein preparation was performed on the downloaded pdb structures essentially to correcting missing hydrogen atoms, ambiguous protonation states, and flapped residues. The ligands were subjected to

Table 3. Validation of Shape Based Queries

PDB	AUC	EF		
		(0.50%)	(1%)	(2%)
2ESM	0.952	108.4	56.61	31.16
2ETK	0.909	53.65	29.34	16.84
3D9V	0.983	134.85	80.70	43.989
3NCZ	0.862	35.54	27.85	22.93
3NDM	0.948	71.30	51.90	32.3
3TV7	0.746	68.08	36.72	22.1
3TWJ	0.811	39.871	21.759	11.977
3V8S	0.947	104.615	55.983	31.947

energy minimization by converging the heavy atoms to RMSD 0.30 Å using OPLS_2005 as force field, after removal of water molecules and subsequently the protein structures were refined. The drug design strategies employed in this study were energy-based pharmacophore and crystal ligand shape-based modeling using protein bound with ligands. These methods were

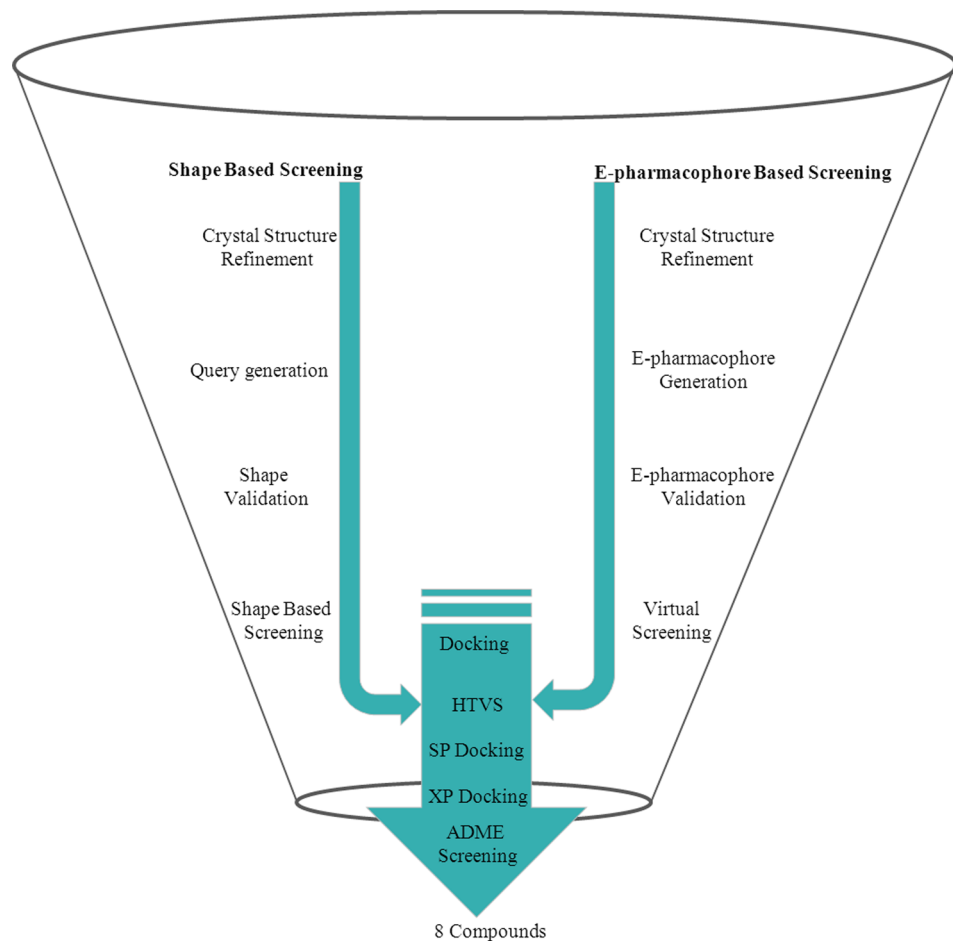


Figure 3. Flowchart of the *in silico* screening process.

considered favorable as they incorporated both the ligand information as well as the protein information along with the favorable contacts with energetic information between the protein and the ligand into the pharmacophore model. All the crystal ligands were redocked onto the prepared protein to generate e-pharmacophore, and the grids utilized for this purpose are presented in the Supporting Information (Table S1). The root-mean-square deviation (rmsd) was less than 1 Å for all 8 crystal ligands. The pharmacophore hypotheses were developed by mapping Glide XP energetic terms onto pharmacophore sites which were calculated based on the structural and energy information between the protein and the ligand. The initial number of pharmacophore sites was set up to ten for all the crystal structures. The total number of pharmacophore sites for each ligand prior to energy-based site selection and the optimized sites for hypothesis generation for the 8 crystal structures of ROCK-I are presented in Figure 1. The crystal ligand from 3V8S gave the maximum pharmacophoric feature of 7 (RRRDDDA), while 3NC2 showed the 6 point feature as RRAADH. Five of the crystal ligands (2ETK, 3D9V, 3NDM, 3TV7, and 3TWJ) showed a 4-point pharmacophore feature among which the features from 2ETK and 3NDM were similar (RRAD). One aromatic (R) and an acceptor (A) features were common in all the eight crystal ligands, and except for 3TWJ all other crystal ligands showed an extra aromatic feature. The distance mapping among the features is presented in Table 1. The distance between the two aromatic features in the aforementioned 7 crystal ligands

was equal (2.45–2.47 Å) except in 3TV7 which was 4.18 Å. Furthermore, most of the common features among the e-pharmacophores showed similar distances except in 3TV7, where R1-R2 and R1-A1 distances were greater. In addition, 3TWJ was missing R1 and A1 features. Overall EF_{1%}, BEDROC, ROC, AUC, and EF_{manual} were then used to measure the overall suitability of the e-pharmacophores (Table 2). The enrichment results for all 8 crystal ligands using the e-pharmacophore method were compared for the enrichment factor (EF1%), BEDROC, based on recovery rate of actives against the ranked decoy database that consisted of 1035 compounds in which 35 were known inhibitors. Based on these values, we selected six out of eight pharmacophores (2ESM, 2ETK, 3D9V, 3NCZ, 3NDM, and 3V8S) for virtual screening as their enrichment values were higher. The structural differences affected their rankings in enrichment calculations (low EF_{1%} and GH scores). Thus, only six e-pharmacophores were selected for virtual screening studies.

In the second model, all eight crystal ligands bound in the active site pocket were subjected to molecular shape analysis using Omega parameters of the OpenEye software, and shapes were created and are presented in Figure 2. These all eight shapes were also validated using the enrichment calculations in which the decoy set consisted of 6319 compounds along with the 35 known ROCK inhibitors (see Table 3). The difference between the two enrichment calculations can be attributed to the way they were generated. E-pharmacophore was considered the only bound pose of the inhibitor, whereas shape-based

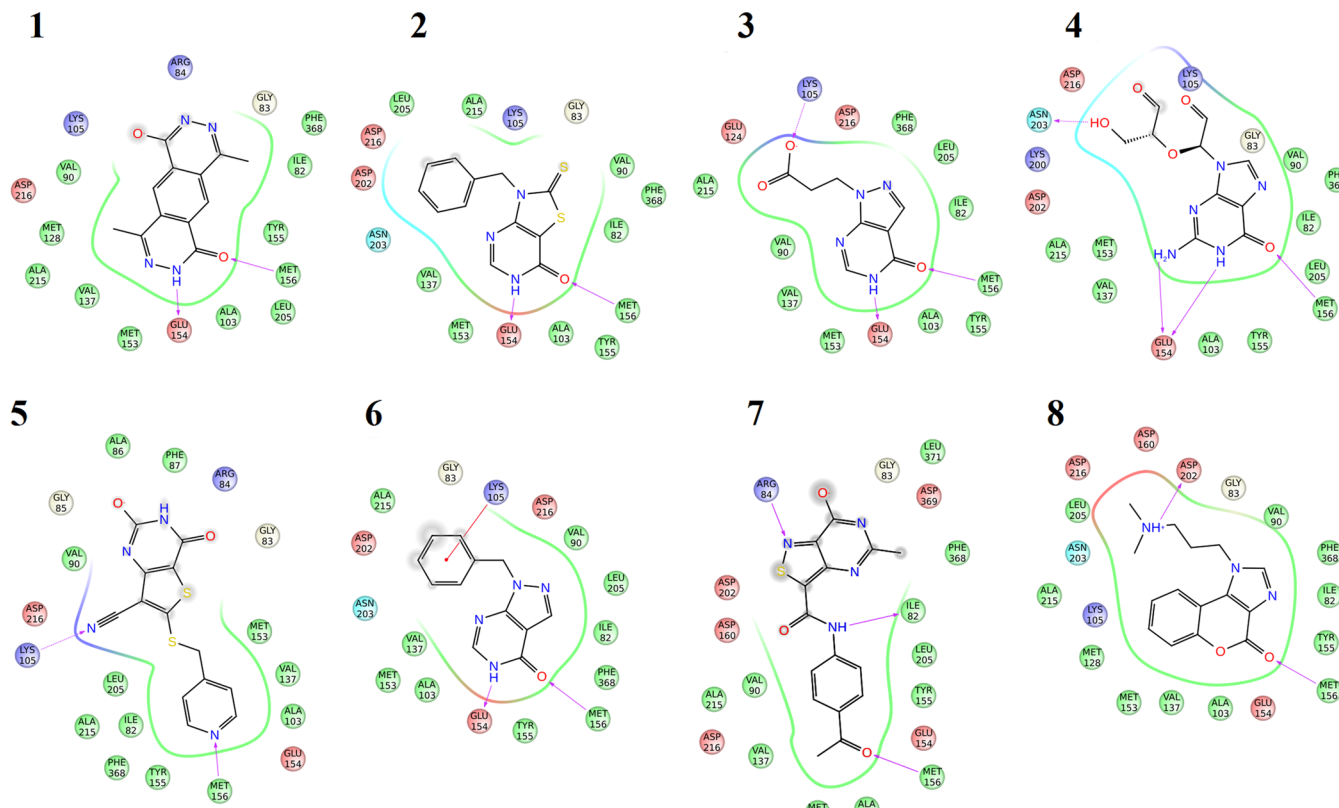


Figure 4. Newly identified ROCK inhibitors and their docking pose in the active site.

Table 4. *In Silico* Parameters (Fitness Score, Tanimoto Combo, GlideScore, Docking Score) and IC₅₀ Value of Selected Compounds

compd no.	fitness	Tanimoto combo	Glide G score	Docking score	IC ₅₀ (μM)
1	2.45	0.581	-7.629	-6.21	17.73
2	2.58	0.481	-8.363	-8.33	4.62
3	2.57	0.541	-8.104	-8.04	5.5
4	2.65	0.48	-7.638	-7.41	3.6
5	2.63	0.576	-6.937	-6.93	6.41
6	2.54	0.483	-7.022	-7.14	2.37
7	2.5	0.794	-7.022	-7.02	2.23
8	2.54	0.48	-6.936	-6.94	1.5

query was based on one of the feasible low energy conformations of the bound ligand. All eight shapes exhibited good enrichment scores and hence were utilized in the virtual screening protocol as presented in Figure 3. This method was based on the crystal ligand-based electrostatic and shape matching protocol within the active site pocket of the protein. In this study we used the programs ROCS and EON (OpenEye Scientific Software, Inc.). The basic goal of any virtual screening protocol is to reduce the enormous virtual chemical space of small organic molecules to a manageable number of compounds that could inhibit the protein. Hence in the present study, virtual screen involved two stages: a preliminary shape matching stage which used carefully validated molecular shape queries based upon each of the eight main active scaffolds, and, in the second strategy, selected e-pharmacophores were utilized as initial filters in the virtual screening protocol. The combination of shape matching and by an e-pharmacophore comparison step for refinement is a relatively

novel approach but has been successfully applied against this target. The output of shape-based and from e-pharmacophore filters was then combined, and the top ligands based on a cutoff value were subjected to docking procedures using various Glide modules (HTVS, SP, and XP docking) as seen in Figure 3. A key advantage to the use of shape-matching and e-pharmacophore filtering as virtual screening strategies was that the actual structure of the crystal ligand may not strongly influence the final hit selection and the use of multiple crystal structures yield diversity in the lead structures as achieved earlier.^{18,19} High-throughput virtual screening was performed with the commercial database (Asinex, www.asinex.com). The library consisted of 525,807 compounds that were then prepared in 3D format and charges assigned using the LigPrep program of Schrodinger, LLC as described in the methods.

Based on docking score and visual inspection, we finally shortlisted 10 compounds which were procured from Asinex for biological evaluation. Interestingly, most of the compounds were either pyrazolopyrimidine analogues or thiazolopyrimidine derivatives. The ROCK-I inhibition assay was performed in a NADH oxidation-phosphate transfer coupled format, as described previously.²⁸ Preliminary screening was conducted at 40 μM compound concentration. Among the 10 compounds tested, only eight showed significant ROCK inhibitory activity at 40 μM (Figure 4) and were further evaluated at serial dilutions to estimate their IC₅₀ values. The activity data along with the computational parameters are presented in Table 4. The structures and the binding mode of all 8 compounds are presented in Figure 4. Among these, compound 8 (1-[3-(dimethylamino)propyl]chromeno[3,4-d]imidazol-4(1H)-one) was the most active with IC₅₀ of 1.5 μM and its structure could be divided into rigid and flexible regions. The rigid region was

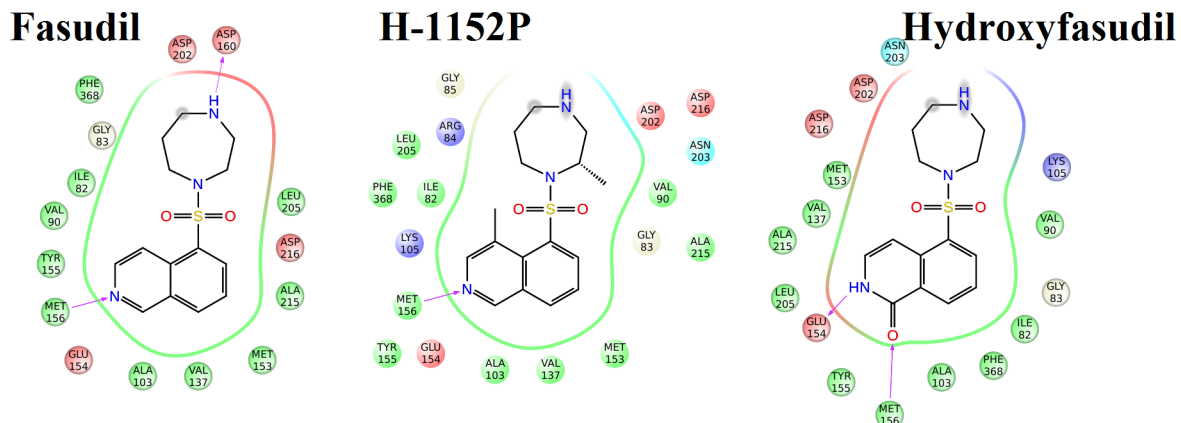


Figure 5. 2D ligand interaction diagrams of Fasudil, H1152, and Hydroxyfasudil with active site residues: Binding pocket characteristics are displayed using color-coded spheres indicating surrounding amino acids, whereas protein–ligand interactions are represented as an arrow in purple. Color coding of amino acids and bonds are explained to the left. These images were generated using the Ligand interaction diagram module of Schrodinger.

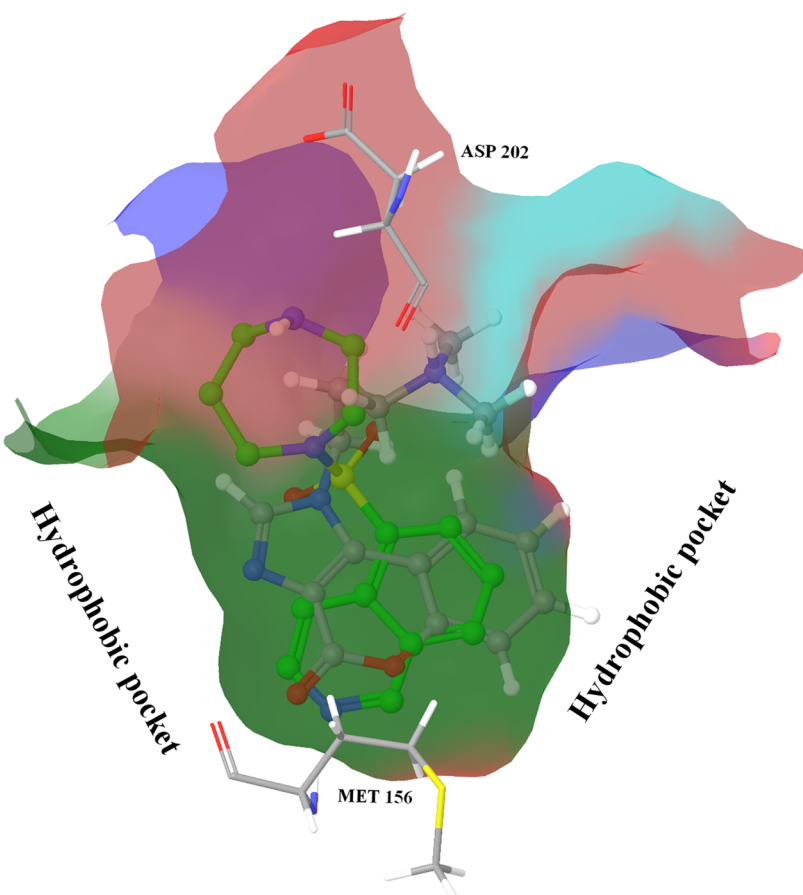


Figure 6. Image showing docked pose of **8** with binding pose of Fasudil. Fasudil binding pose is shown in green. Molecular surface of 2ESM active site is shown and is colored according to amino acid properties. The green portion of the pocket is lined by hydrophobic residues; red is lined by residues bearing negative charge, and blue indicates molecular surface belonging to positively charged residues.

planar and made up of three rings of chromeno[3,4-*d*]imidazol-4(1*H*)-one moiety, and the flexible dimethylaminopropyl group in the tail region was oriented toward the hydration site of the active site pocket. Compound **8** formed two hydrogen bonds with the protein. The oxygen atom present in the rigid portion acted as a hydrogen bond acceptor and formed a hydrogen bond with N of Met156, which acted as a hydrogen bond donor. Another hydrogen bond was formed between the lone pair of the N atom of the dimethylamino group of the flexible

region which acts as a hydrogen bond donor and forms a hydrogen bond with an O atom of Asp202. Fasudil, a known ROCK inhibitor, employed as standard also showed the same hydrogen bonds with Met156 and Asp202, whereas the other known inhibitors like H1152 and Hydroxyfasudil showed interactions with Met156 (Figure 5). All other compounds showed IC₅₀ less than 10 μ M except for compound **1**, which displayed an IC₅₀ of 17.73 μ M.

Table 5. ADME Properties of Hits in Comparison with Fasudil

compd	MW	Qplog Po/w	QplogS	Qplog HERG	QPP Caco	QP logBB	QPP MDCK	QPlogKp	oral absorption	% human oral absorption	rule of five
1	241.2	-1.924	-1.324	-3.815	5.841	-2.879	1.906	-6.826	2	29.397	0
2	275.3	2.01	-3.264	-4.671	990.1	-0.23	1688	-2.42	3	92.334	0
3	208.2	-0.08	-1.411	-1.834	23.74	-1.371	11.04	-4.791	2	51.096	0
4	281.2	-2.513	-0.892	-3.977	6.237	-2.908	2.046	-6.749	2	26.46	0
5	316.4	0.996	-4.226	-4.796	50.21	-1.768	47.15	-4.81	3	63.218	0
6	272.3	0.595	-0.62	-4.971	119.4	-0.489	55.03	-5.255	2	67.603	0
7	328.3	1.76	-4.089	-5.373	115.6	-1.614	90.28	-4.297	3	74.176	0
8	271.3	0.992	-0.309	-4.412	234.3	-0.131	114	-4.569	3	75.168	0
Fasudil	291.3	0.768	-1.314	-5.015	249.5	-0.039	122.1	-4.586	2	74.346	0

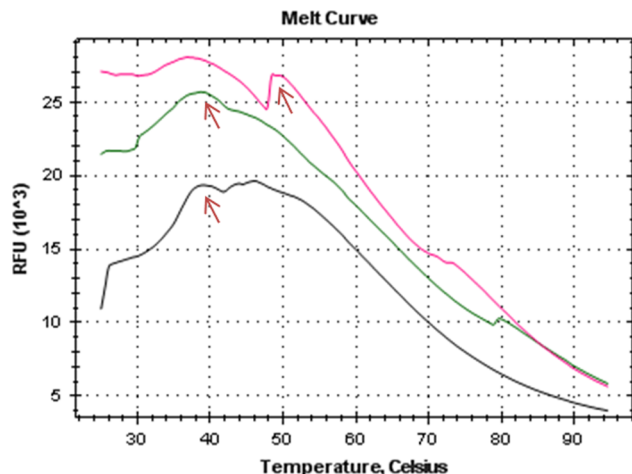


Figure 7. Stabilization of ROCK-inhibitor complexes as measured by differential scanning fluorimetry. Native ROCK (green) and ROCK in the presence of Fasudil (black); compound 8 (pink). Arrows indicate the inflection temperatures.

Table 6. Activity of Compounds in IMR-32 Cells

compd code	HEK 293 cell lines		IMR-32 cell lines		
	percent cytotoxicity (100 μ M)	GI ₅₀ (μ M)	ROS IC ₅₀ ^a	clonogenic (SF)	
1	34.00	0.02	6.24	66.67	
2	44.83	0.05	4.13	66.67	
3	52.30	0.33	4.55	0.47	
4	31.88	34.03	5.49	0.99	
5	50.57	0.89	4.89	143.51	
6	47.21	0.70	4.40	169.41	
7	73.70	0.20	5.25	78.67	
8	14.23	0.27	5.80	79.25	
Fasudil	30.00	0.02	4.96	60.63	

^aIC₅₀ for ROS inhibition.

Comparison of the docked poses of the eight inhibitors revealed that compound 8 occupied the maximum pocket volume among the eight compounds. The rings of compounds 1–7 occupied the hydrophobic pocket with near vertical orientation, whereas the rings of 8 were aligned in a horizontal direction. Due to this unusual conformation, the hydrophobic rings of 8 were well oriented in the hydrophobic cavity of the active site pocket, leading to enhanced hydrophobic interactions. In addition, the docked pose of 8 was quite similar to that of Fasudil as is evident from Figure 6. Hence, the orientation of the hydrophobic rings toward the hydrophobic region with good occupancy and orientation of polar tail

Table 7. Anti-HCV Activity and Cell Viability of Compounds 1–8

compd code	CC ₅₀ (μ M) ^a	Huh7/Rep-Feo1b (% inhibition) ^b	Huh7.5-FGR-JC1-Rluc2A (% inhibition) ^c
1	>224	NI ^d	55 ± 6
2	>224	23 ± 10	35 ± 3
3	180	51 ± 13	85 ± 2
4	>224	NI ^d	38 ± 10
5	>224	38 ± 3	31 ± 2
6	96	91 ± 2	70 ± 2
7	>224	NI ^d	NI ^d
8	>224	59 ± 4	19 ± 10

^aCC₅₀ values were evaluated in Huh 7.5 parental cells by the MTS assay. ^bHuh7/Rep-Feo1b were treated with the indicated compounds at 50 μ M concentration for 48 h, and the inhibitory effect of the compound on HCV RNA replication was determined by the relative luciferase activity in compound treated versus DMSO controls.

^cHuh7.5-FGR-JC1-Rluc2A reporter cells were treated with the indicated compounds at 50 μ M concentration for 48 h and the inhibitory effect of the compound on HCV RNA replication was determined by the relative luciferase activity in compound treated versus DMSO controls. The data represents an average of three independent experiments with standard deviation. ^dNI; no inhibition.

toward the hydrophilic site justified the bioactivity of compound 8 compared to the others (1–7).

Of the eight inhibitors, compound 8 was of special interest, not only because of its highest ROCK inhibitory activity in this study but also for its interesting conformation. Alignment of compound 8 with Fasudil not only showed perfect overlap of the rigid rings but also the tail region containing the dimethylamine group aligned to the homopiperazine ring of Fasudil. In addition, higher potency of 8 may be attributed to the greater extent of its hydrophobic interactions in the active site pocket. Interestingly, 8 shared more similarities with Fasudil as it also showed similar calculated ADME properties (Table 5). Almost all compounds exhibited acceptable oral absorption, and there were no violations of Lipinski's rule of five.³⁶ These results suggest that these compounds may be suitable for oral dosing and topical application. In addition, they may serve as a template for further lead modification and optimization.

The interaction of the most potent compound 8 with ROCK was further evaluated by measuring the thermal stability of the protein–ligand complex employing DSF biophysical experiments. Experiments with ROCK-I in complex with Fasudil were also performed for comparison. The DSF approach measures the melting temperature (T_m) of a protein as an indicator of its thermal stability, and an increase in T_m indicates higher stability. Figure 7 shows the melting curve (T_m) of ROCK-I

alone and in complex with compounds **8** or Fasudil. Native ROCK exhibited a T_m of 35.3 °C, which increased to 49.4 °C ($\Delta T_m = +14.1$ °C) upon compound **8** (100 μM) binding, in contrast to no change observed upon Fasudil (75 μM) binding ($T_m = 35.8$ °C). Thus, the higher T_m of ROCK-**8** protein-ligand complex relative to ROCK alone signified a stabilization of ROCK upon **8** binding, thus accounting for its more potent inhibition.

Methylmercury (MeHg) is a well-known environmental neurotoxicant implicated in neuropathological changes. Previous studies have demonstrated that inhibition of the Rho/ROCK pathway prevented MeHg-induced intoxication of neuronal cells.³⁷ In another study, MeHg exposure down-regulated the expression of Rac1 and RhoA causing axonal degeneration and apoptosis of cultured cortical neuronal cells.³⁸ In this present study, we therefore utilized IMR-32 neuroblastoma cells treated with MeHg, as models to evaluate the effect of the eight ROCK inhibitors. The compounds were also analyzed in cell based assays for their cytotoxicity parameters and ability to inhibit of reactive oxygen species. The results are presented in Table 6. Compound **8** exhibited promising activity in inhibiting the MeHg-induced neurotoxicity of IMR-32 neuroblastoma cells resulting from the overexpression of ROCK and in quenching reactive oxygen species generated upon MeHg treatment. Surprisingly compound **1** which showed lower activity in the enzyme assay also exhibited equipotent activity as Fasudil. In the cytotoxicity assay, all compounds except **3**, **5**, and **7** exhibited no or negligible toxicity at 100 μM . Clonogenic assay is reported as the method of choice to determine cell reproductive death after treatment with cytotoxic agents to determine their effectiveness.³⁹ Hence the compounds were also evaluated in the clonogenic assay which indicated that all the compounds except **3** and **4** showed cytoprotective activity and were better than Fasudil.

In parental Huh7 hepatoma cells, all compounds exhibited negligible cytotoxicity (Table 7). Of these, **3** and **6** exhibited CC_{50} values of 180 μM and 96 μM , respectively, while all others displayed ≥ 224 μM CC_{50} values. Previous studies have explored ROCK inhibitors as probes for unraveling HCV pathogenesis.^{13,14,40,41} We were therefore curious to investigate the effect of the 8 ROCK inhibitors on HCV RNA replication. With the exception of **1** and **7**, all compounds exhibited inhibition of HCV RNA replication, albeit to varying extents depending on the compound and HCV genotype. In genotype 1, this ranged from 23 to 91%, while in genotype 2, 19 to 85% inhibition was observed at 50 μM compound concentration. Notably, **7** displayed no inhibition in both genotypes, while **1** inhibited genotype 2 by 55% at 50 μM in contrast to genotype 1 which displayed no inhibition at this concentration. Together, this data indicates the utility of our identified leads for further development as anti-HCV agents.

3. CONCLUSION

In the present study structure-based e-pharmacophore and shape-based matching were employed to identify structurally diverse, small molecule inhibitors of ROCK1 useful in the treatment of neuronal disorders and suppressing HCV RNA replication. Eight promising compounds were identified as prototypical leads with compound **8** emerging as the most active in vitro ROCK inhibitor. In cell based assays, several of these compounds were also found to be effective in growth and ROS inhibition. Furthermore, the compounds displayed some utility in inhibiting HCV RNA replication in cell based assays.

Thus, these eight molecule scaffolds can be utilized as promising leads for further optimization and development as ROCK inhibitors.

■ ASSOCIATED CONTENT

■ Supporting Information

Text, references, and Table S1. This material is available free of charge via the Internet at <http://pubs.acs.org>.

■ AUTHOR INFORMATION

Corresponding Authors

*N.K.-B.: Phone: 973-972-8653. Fax: 973-972-5594. E-mail: kaushik@njms.rutgers.edu.

*P.Y.: Phone: 91-40-66303515. Fax: +91-40-66303998. E-mail: pyogee@hyderabad.bits-pilani.ac.in.

Author Contributions

R.K.M. and R.A. contributed equally.

Notes

The authors declare no competing financial interest.

■ ACKNOWLEDGMENTS

R.K.M. thanks the Council of Scientific and Industrial Research (CSIR), Government of India, for fellowship. R.A. thanks the Institute fellowship provided by the host institute. The authors would like to acknowledge Mr. Madhu Babu Battu for his support.

■ ABBREVIATIONS

ADME, “Absorption, Distribution, Metabolism, Elimination”; AUC, area under curve; BEDROC, Boltzmann-enhanced discrimination of receiver operating characteristic; DSF, differential scanning fluorimetry; DUD, directory of useful decoys; EF, enrichment factor; GH, goodness of hit; HTVS, high throughput virtual screening mode of docking; MeHg, methyl mercury; MTT, ((3-(4,5-dimethylthiazol-2-yl)-2,5-diphenyltetrazolium bromide); PDB, Protein Data Bank; ROC, receiver operating characteristics; ROCK, rho kinase enzyme; SP, standard precision docking mode; XP, extra precision docking mode

■ REFERENCES

- (1) Nakagawa, O.; Fujisawa, K.; Ishizaki, T.; Saito, Y.; Nakao, K.; Narumiya, S. ROCK-I and ROCK-II, two isoforms of Rho-associated coiled-coil forming protein serine/threonine kinase in mice. *FEBS Lett.* **1996**, 392 (2), 189–193.
- (2) Fukata, Y.; Amano, M.; Kaibuchi, K. Rho-Rho-kinase pathway in smooth muscle contraction and cytoskeletal reorganization of non-muscle cells. *Trends Pharmacol. Sci.* **2001**, 22, 32–39.
- (3) Mammoto, A.; Huang, S.; Moore, K.; Oh, P.; Ingber, D. E. Role of RhoA, mDia, and ROCK in cell shape-dependent control of the Skp2-p27kip1 pathway and the G1/S transition. *J. Biol. Chem.* **2004**, 279, 26323–26330.
- (4) Wirth, A. Rho kinase and hypertension. *Biochim. Biophys. Acta* **2010**, 1802, 1276–84.
- (5) Shin, H. K.; Salomone, S.; Ayata, C. Targeting cerebrovascular Rho-kinase in stroke. *Expert Opin. Ther. Targets* **2008**, 12 (12), 1547–64.
- (6) Colligris, B.; Crooke, A.; Huete, F.; Pintor, J. Potential role of Rho-associated protein kinase inhibitors for glaucoma treatment. *Recent Pat. Endocr., Metab. Immune Drug Discovery* **2012**, 6 (2), 89–98.
- (7) Mali, R. S.; Ramdas, B.; Ma, P.; Shi, J.; Munugalavadla, V.; Sims, E.; Wei, L.; Vemula, S.; Nabinger, S. C.; Goodwin, C. B.; Chan, R. J.; Traina, F.; Visconte, V.; Tiu, R. V.; Lewis, T. A.; Stern, A. M.; Wen, Q.; Crispino, J. D.; Boswell, H. S.; Kapur, R. Rho kinase regulates the

- survival and transformation of cells bearing oncogenic forms of KIT, FLT3, and BCR-ABL Cancer. *Cell* **2011**, *20*, 357–69.
- (8) Rangasamy, S.; McGuire, P. G.; Das, A. Diabetic retinopathy and inflammation: novel therapeutic targets. *Middle East. J. Ophthalmol.* **2012**, *19*, 52–9.
- (9) Komers, R. Rho kinase inhibition in diabetic nephropathy. *Curr. Opin. Nephrol. Hypertens.* **2011**, *20* (1), 77–83.
- (10) Gratzke, C.; Strong, T. D.; Gebka, M. A.; Champion, H. C.; Stief, C. G.; Burnett, A. L.; Bivalacqua, T. J. Activated RhoA/Rho kinase impairs erectile function after cavernous nerve injury in rats. *J. Urol.* **2010**, *184* (5), 2197–204.
- (11) Tatsumi, S.; Mabuchi, T.; Katano, T.; Matsumura, S.; Abe, T.; Hidaka, H.; Suzuki, M.; Sasaki, Y.; Minami, T.; Ito, S. Involvement of Rho-kinase in inflammatory and neuropathic pain through phosphorylation of myristoylated alanine-rich C-kinase substrate (MARCKS). *Neuroscience* **2005**, *131* (2), 491–8.
- (12) Mishra, R. K.; Alokam, R.; Sriram, D.; Yogeeshwari, P. Potential role of Rho Kinase inhibitors in combating diabetes-related complications including diabetic neuropathy—a review. *Curr. Diabetes Rev.* **2013**, *9* (3), 249–66.
- (13) Christopher, J. M.; Helen, J. H.; Michelle, J. F.; Garrick, W.; Gary, R.; Christopher, D.; Sven, C. D.; van, I.; Peter, B.; Jane, A. M. Polarization restricts Hepatitis C virus entry into HepG2 hepatoma cells. *J. Virol.* **2009**, *83* (12), 6211–6221.
- (14) Kah, J.; Schrader, J.; Wustenberg, A.; Tiegs, G.; Sass, G. Matrix stiffness modulates inhibition of HCV replication by Fluvastatin in vitro. *Z. Gasteroenterol.* **2013**, *51*, 5–28.
- (15) Jacobs, M.; Hayakawa, K.; Swenson, L.; Bellon, S.; Fleming, M.; Taslimi, P.; Doran, J. The structure of dimeric ROCK I reveals the mechanism for ligand selectivity. *J. Biol. Chem.* **2006**, *281* (1), 260–268.
- (16) Ortiz-Sanchez, J. M.; Nichols, S. E.; Sayyah, J.; Brown, J. H.; McCammon, J. A.; Grant, B. J. Identification of Potential Small Molecule Binding Pockets on Rho Family GTPases. *PLoS One* **2012**, *7* (7), e40809.
- (17) Li, R.; Martin, M. P.; Liu, Y.; Wang, B.; Patel, R. A.; Zhu, J. Y.; Sun, N.; Pireddu, R.; Lawrence, N. J.; Li, J.; Haura, E. B.; Sung, S. S.; Guida, W. C.; Schonbrunn, E.; Sebti, S. M. Fragment-based and structure-guided discovery and optimization of Rho kinase inhibitors. *J. Med. Chem.* **2012**, *55* (5), 2474–8.
- (18) Palakurti, R.; Sriram, D.; Yogeeshwari, P.; Vadrevu, R. Multiple e-Pharmacophore Modeling Combined with High-Throughput Virtual Screening and Docking to Identify Potential Inhibitors of β -Secretase(BACE1). *Mol. Inf.* **2013**, *32*, 385–398.
- (19) Therese, P. J.; Manver, D.; Kondepudi, S.; Battu, M. B.; Sriram, D.; Basu, A.; Yogeeshwari, P.; Kaushik-Basu, N. Multiple e-pharmacophore modeling, 3D-QSAR and high-throughput virtual screening of Hepatitis C virus NSSB polymerase inhibitors. *J. Chem. Inf. Model.* **2014**, *54* (2), 539–552.
- (20) Glide, version 5.7; Schrödinger, LLC: New York, NY, 2011.
- (21) Zweig, M. H.; Campbell, G. Receiver-operating characteristic (ROC) plots: a fundamental evaluation tool in clinical medicine. *Clin. Chem.* **1993**, *39* (4), 561–77.
- (22) Qin, J.; Lei, B.; Xi, L.; Liu, H.; Yao, X. Molecular modeling studies of Rho kinase inhibitors using molecular docking and 3D-QSAR analysis. *Eur. J. Med. Chem.* **2010**, *45* (7), 2768–76.
- (23) Huang, N.; Shoichet, B. K.; Irwin, J. J. Benchmarking sets for molecular docking. *J. Med. Chem.* **2006**, *49* (23), 6789–801.
- (24) LigPrep, version 2.5; Schrödinger, LLC: New York, NY, 2012.
- (25) Omega, version 2.3.2; Openeye Scientific Software Inc.: Santa Fe, 2009.
- (26) Pratim Roy, P.; Paul, S.; Mitra, I.; Roy, K. On two novel parameters for validation of predictive QSAR models. *Molecules* **2009**, *14*, 1660–701.
- (27) Qikprop, version 3.4; Schrodinger, LLC: New York, NY, 2011.
- (28) Doran, J. D.; Jacobs, M. D. ROCK enzymatic assay. *Methods Mol. Biol.* **2008**, *468*, 197–205.
- (29) Niesen, F. H.; Berglund, H.; Vedadi, M. The use of differential scanning fluorimetry to detect ligand interactions that promote protein stability. *Nat. Protoc.* **2007**, *2*, 2212–2221.
- (30) Plumb, J. A. Cell sensitivity assays: the MTT assay. *Cancer Cell Culture*; Springer: 2004; pp 165–69.
- (31) Eruslanov, E.; Kusmartsev, S. Identification of ROS using oxidized DCFDA and flow cytometry. *Methods Mol. Biol.* **2010**, *594*, 57–72.
- (32) Munshi, A.; Hobbs, M.; Meyn, R. E. Clonogenic cell survival assay. *Methods Mol. Med.* **2005**, *110*, 21–28.
- (33) Kim, K.; Kim, K. H.; Kim, H. Y.; Cho, H. K.; Sakamoto, N.; Cheong, J. Curcumin inhibits hepatitis C virus replication via suppressing the Akt-SREBP-1 pathway. *FEBS Lett.* **2010**, *584*, 707–712.
- (34) Nichols, D. B.; Fournet, G.; Gurukumar, K. R.; Basu, A.; Lee, J. C.; Sakamoto, N.; Kozelski, F.; Musmuca, I.; Joseph, B.; Ragni, R.; Kaushik-Basu, N. Inhibition of hepatitis C virus NSSB polymerase by S-trityl-L-cysteine derivatives. *Eur. J. Med. Chem.* **2012**, *49*, 191–9.
- (35) Küçükgüzel, I.; Satılmış, G.; Gurukumar, K. R.; Basu, A.; Tatar, E.; Nichols, D. B.; Talele, T. T.; Kaushik-Basu, N. 2-Heteroarylimino-5-arylidene-4-thiazolidinones as a new class of non-nucleoside inhibitors of HCV NSSB polymerase. *Eur. J. Med. Chem.* **2013**, *69*, 31–41.
- (36) Lipinski, C. A.; Lombardo, F.; Dominy, B. W.; Feeny, P. J. Experimental and computational approaches to estimate solubility and permeability in drug discovery and development settings. *Adv. Drug Delivery Res.* **2001**, *46*, 3–26.
- (37) Fujimura, M.; Usuki, F.; Kawamura, M.; Izumo, M. Inhibition of the Rho/ROCK pathway prevents neuronal degeneration *in vitro* and *in vivo* following methylmercury exposure. *Toxicol. Appl. Pharmacol.* **2011**, *250*, 1–9.
- (38) Fujimura, M.; Usuki, F.; Sawada, M.; Rostene, W.; Godefroy, D.; Takashima, A. Methylmercury exposure downregulates the expression of Rac1 and leads to neuritic degeneration and ultimately apoptosis in cerebrocortical neurons. *Neurotoxicology* **2009**, *30*, 16–22.
- (39) Franken, N. A.; Rodermond, H. M.; Stap, J.; Haveman, J.; van Bree, C. Clonogenic assays of cell *in vitro*. *Nat. Protoc.* **2006**, *1*, 2315–2319.
- (40) Bauer, A. F.; Sonzogni, S.; Meyer, L.; Zeuzem, S.; Piiper, A.; Biondi, R. M.; Neimanis, S. Regulation of protein kinase C-related protein kinase 2 (PRK2) by an intermolecular PRK2-PRK2 interaction mediated by its N-terminal domain. *J. Biol. Chem.* **2012**, *287*, 20590–205602.
- (41) Kim, S. J.; Kim, J. H.; Sun, J. M.; Kim, M. G.; Oh, J. W. Suppression of hepatitis C virus replication by protein kinase C-related kinase 2 inhibitors that block phosphorylation of viral RNA polymerase. *J. Viral. Hepat.* **2009**, *16*, 697–704.